Passivation of Sponge Iron and GAC in Fe 0 /GAC Mixed-Potential Corrosion Reactor

DATASET *in* INDUSTRIAL & ENGINEERING CHEMISTRY RESEARCH · MAY 2012

Impact Factor: 2.59 · DOI: 10.1021/ie203019t

3 AUTHORS, INCLUDING:

Bo Lai
Sichuan University
25 PUBLICATIONS **196** CITATIONS
SEE PROFILE

Ping Yang
45 PUBLICATIONS **842** CITATIONS
SEE PROFILE

I&EC research
Industrial & Engineering Chemistry Research

Article

pubs.acs.org/IECR

Passivation of Sponge Iron and GAC in Fe^0/GAC Mixed-Potential Corrosion Reactor

Bo Lai,[†,‡,*] Yuexi Zhou,[‡] and Ping Yang[†]

[†]Department of Environmental Science and Engineering, School of Architecture and Environment, Sichuan University, Chengdu 610065, China

[‡]Research Center of Water Pollution Control Technology, Chinese Research Academy of Environmental Sciences, Beijing 100012, China

Supporting Information

ABSTRACT: The Fe^0/GAC mixed-potential corrosion reactor was used to treat the complicated, toxic, and refractory ABS resin wastewater. In the 100 days continuous run, the effect of the packing particles passivation on the treatment efficiency of the Fe^0/GAC mixed-potential corrosion reactor was investigated seriously. The formation mechanism of the compounds in passive film was investigated first by SEM, EDS, and X-ray dot-mapping, which was the precondition for the control of the passivation of packing particles. The results show that the passive film consisted of five kinds of compounds such as $Fe_3(PO)_2{\cdot}8H_2O$, $FePO_4{\cdot}3H_2O$, Fe_2O_3, Fe_3O_4, and FeS, which obstructed the formation of macroscopic galvanic cells between sponge iron (Fe^0) and GAC and decreased the COD treatment efficiency of the Fe^0/GAC mixed-potential corrosion reactor from 45 to 55% to 0%. The formation of passive film mainly resulted from the elements of S and P, which were from the SO_4^{2-} and PO_4^{3-} in ABS resin wastewater. Therefore, the inorganic ions in wastewater, especially for SO_4^{2-} and PO_4^{3-}, should be removed first before the treatment of the Fe^0/GAC mixed-potential corrosion reactor.

1. INTRODUCTION

In China, most of the acrylonitrile−butadiene−styrene (ABS) resin manufacturers use emulsion grafting-blend production technology to produce various types of ABS resin.[1] With this production technology, acrylonitrile, butadiene, styrene, and hundreds of auxiliary agents are needed in the whole production process, which leads to complicated, toxic, and refractory ABS resin wastewater.[2] Thus, the ABS resin wastewater is one of the typical high-strength petrochemical wastewaters. If the untreated wastewater is discharged into the receiving water directly, it will cause profound damage to the environment. The conventional treatment methods including ozonation,[3−6] electro-Fenton,[7−9] and three-dimensional electrodes[10] can be used to treat this wastewater. Nevertheless, all of these treatment technologies suffer the limitations of high costs. Therefore, it is necessary to develop an effective, robust, and economically feasible treatment technology for the ABS resin wastewater.

In recent years, zerovalent iron (ZVI) has attracted increasing interest for the treatment of toxic refractory wastewater such as bromoamine acid wastewater,[11] liquid crystal display (LCD) manufacturing wastewater,[12] nitrobenzene wastewater,[13,14] olive mill wastewater,[15] and coking wastewater.[16] The ZVI has been proven to be a cost-effective treatment approach for toxic refractory wastewater. The pollutant degradation efficiency of the ZVI would be influenced by the type and number of cathode. Granular activated carbon (GAC) is added as cathode into the ZVI system, which changes the ZVI system into a Fe^0/GAC mixed-potential corrosion reactor. Then a large number of macroscopic galvanic cells are formed by the contact of Fe^0 and GAC, which can improve the current efficiency of the internal electrolysis significantly.[17,18] The half-cell reactions of the Fe^0/GAC mixed-potential corrosion reactor can be represented as follows:

Cathode (reduction)

Acidic:

$$2H^+ + 2e^- \rightarrow 2[H] \rightarrow H_2\uparrow \qquad E^\theta(H^+/H_2) = 0.00V \tag{1}$$

Acid with oxygen:

$$O_2 + 4H^+ + 4e^- \rightarrow 2H_2O \qquad E^\theta(O_2/OH^-) = 1.23V \tag{2}$$

Neutral to alkaline:

$$O_2 + 2H_2O + 4e^- \rightarrow 4OH^- \qquad E^\theta(O_2/OH^-) = 0.40V \tag{3}$$

Anode (oxidation)

$$Fe - 2e^- \rightarrow Fe^{2+} \qquad E^\theta(Fe^{2+}/Fe) = -0.44V \tag{4}$$

Received: December 23, 2011
Revised: April 18, 2012
Accepted: May 3, 2012
Published: May 3, 2012

It is clear that organic pollutants can be reduced by [H] produced from electrode action in Fe^0/GAC mixed-potential corrosion reactor.[19] Furthermore, organic pollutants can also be removed by adsorption, enmeshment, and coprecipitation[17] by the ferric and ferrous hydroxides formed from oxidation and precipitation of Fe^{2+}. Zee et al.[20] discovered that GAC could improve the reduction by accepting electrons and transferring the electrons to pollutants. Meanwhile, GAC was chosen as cathode because of its strong physical adsorption, and activated carbon can adsorb some of the organic pollutants, especially for the hydrophobic ones.[17] In other words, the GAC could enhance the resistance to the shock loadings of toxic refractory wastewater by its strong high physical adsorption.

Both ZVI and Fe^0/GAC systems are the cost-effective treatment approaches for toxic and refractory wastewater, but they both will loss their reactivity over time which results from the corrosion products or other precipitates on the surface of the Fe^0 and GAC.[21] In other words, the operating life of the ZVI and Fe^0/GAC systems is not long enough for the treatment of wastewater. Liu et al.[21] used ultrasound to prolong the operating life of a Fe^0/GAC mixed-potential corrosion reactor, but the reactor could not overcome the passivation of Fe^0 and GAC completely. Moreover, it would consume energy and increase the operating cost. Therefore, it is necessary to develop a cost-effective and robust Fe^0/GAC mixed-potential corrosion reactor for the treatment of toxic and refractory wastewater.

In this study, ABS resin wastewater was treated by the Fe^0/GAC mixed-potential corrosion reactor, and the formation mechanism of passive film on the surface of Fe^0 and GAC in the Fe^0/GAC mixed-potential corrosion reactor after the long-term run was investigated in detail. Effects of PO_4^{3-} and SO_4^{2-} on the formation of passive film on the surface of Fe^0 and GAC were studied in the treatment process of the Fe^0/GAC mixed-potential corrosion reactor.

2. MATERIALS AND METHODS

2.1. Raw Wastewater. The wastewater used in this study was obtained from a petrochemical industry in north China. The main physicochemical characteristics of ABS resin wastewater are listed in Table S1 (Supporting Information).

2.2. Fe^0/GAC Mixed-Potential Corrosion. The experimental apparatus was a cylindrical mixed-potential corrosion reactor (Φ10 cm × 50 cm) (see Figure S1, Supporting Information). The reactor was made of transparent synthetic glass columns. The granular activated carbon (GAC) and sponge iron (Fe^0) were mixed together with a volumetric ratio of 1:1, and then packed in the reactor as a fixed bed with a bed height of 40 cm. A commercial sponge iron was obtained from Beijing MingJian Technology Company. It has a mean particle size of approximately 3−5 mm and a bulk densities of 3 $g \cdot cm^{-3}$. The main element of the sponge iron is Fe (>98%), and the residual elements in the sponge iron are Si, Mn, Ca, C, Mg, and Al (<2%) (see Figure S2, Supporting Information). From a macroscopic perspective, the surface morphology of sponge iron particles is sponginess, and there are a plenty of big gaps on the surface of a sponge iron particle (see Figure S3a, Supporting Information). However, there is no pore on the surface of sponge iron from a micrometer aspect (see Figure S3b, Supporting Information). Commercial granular activated carbon (GAC) from Beijing KeCheng GuangHua New Technology Company was used in this study. It has mean particle size of 3−5 mm, a specific surface of 748 $m^2 \cdot g^{-1}$ according to the BET method, a total pore volume of 0.481 $mL \cdot g^{-1}$, and a bulk density of 0.493 $g \cdot cm^{-3}$. There are some cracks and big pores on the surface of GAC (see Figure S3cd, Supporting Information).

2.3. Experimental Methods. The pH of the ABS resin wastewater was adjusted to 4.0 using diluted sulfuric acid (10%) or sodium hydroxide solutions (5 mol L^{-1}). The hydraulic retention time (HRT) of the Fe^0/GAC mixed-potential corrosion reactor was 4 h, and the temperature of the batch was kept at about 25 °C. The reactors were operated continuously 100 days at a constant hydraulic retention time (HRT) of 4 h, and the COD, PO_4^{3-}, and total iron of the effluent were determined each day. After 100 days run, the characteristics of passive Fe^0 and GAC were analyzed by scanning electron microscope (SEM), energy dispersive spectrometer (EDS), X-ray diffraction (XRD), and specific surface area measuring instrument, respectively.

2.4. Sample Preparation and Analytical Methods. Energy dispersive spectrometry (EDS) analysis was performed by a permanent thin film window link (Oxford Instruments) detector and WinEDS software in a Hitachi S-3500N scanning electron microscope (SEM) using an electron beam operating voltage of 25 kV and emission current of 60−70 μA. The EDS was used to analyze elements on the surface of the sponge iron and GAC. The Hitachi S-3500N SEM was used to observe the morphologies of the sponge iron and GAC. To investigate the element distribution on the cross-section of sponge iron and GAC, the sponge iron and GAC was fixed by epoxy resins, then the fixed sponge iron and GAC was split from the middle by the cutting machine, and their cross-section should be polished before detection. At last, the X-ray dot-mapping was used to characterize the element distribution at the cross-section of the sponge iron and GAC. A Phillips Xpert Pro diffractometer with a Cu Kα radiation source (λ = 1.5406 Å) was used for XRD analysis (generator voltage of 40 keV; tube current of 30 mA). XRD spectra were acquired between 2θ of 4−85, with a step size of 0.05 and a 2 s dwell time. Analysis of the surface physical properties of the sponge iron and GAC includes determination of the pore size distribution, total surface area, and total pore volume. Pore size distribution, total surface area, and total pore volume of the sponge iron and GAC were determined from N_2 adsorption and desorption isotherms using a specific surface area measuring instrument (Nova 4200, Quantachrome Instruments, UK). Total surface area was calculated using a BET mathematical model, and the total pore volume and pore size distribution were identified using the t-plot and BJH method. Before the adsorption process commences, all the samples were outgassed for 5 h at 300 °C, in order to remove previously adsorbed gases from the surface. The chemical oxygen demand (COD) and biochemical oxygen demand (BOD_5) were determined using a COD analyzer (Hach, USA) and respirometer (OxiTop IS12, WTW, Germany), respectively. PO_4^{3-} and SO_4^{2-} were determined by ion chromatography (ICS-1000, Dionex, USA). Total iron of the effluent was determined by atomic absorption spectrometry (AA-6300, Shimadzu, Japan). The pH was measured by a pHS-3C pH Meter (Rex, China).

3. RESULTS AND DISCUSSION

3.1. Treatment Efficiency of the Fe^0/GAC Mixed-Potential Corrosion Reactor. The COD and PO_4^{3-} concentrations of the raw ABS resin wastewater were about 1200 and 55 mg L^{-1}, respectively. Figure 1a shows the time

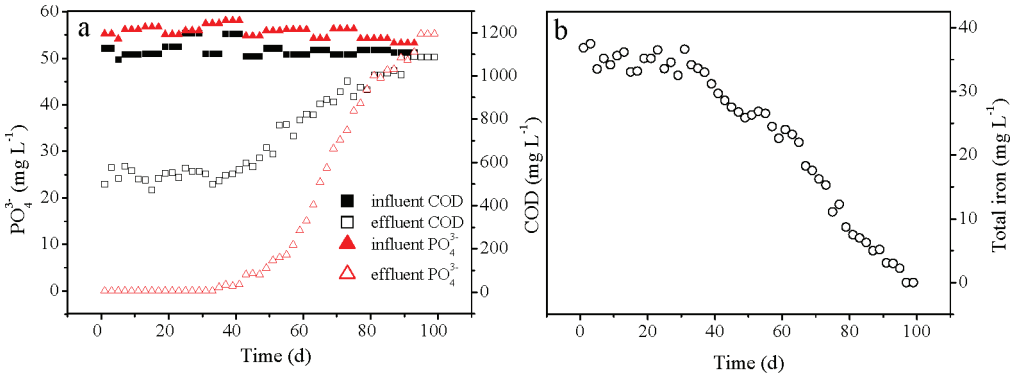

Figure 1. Changes of effluent quality of Fe^0/GAC mixed-potential corrosion reactor (a) COD and PO_4^{3-}; (b) total iron.

history of COD and PO_4^{3-} concentration of the ABS resin wastewater after treatment by the Fe^0/GAC mixed-potential corrosion reactor. During the first 40 days, the COD and PO_4^{3-} concentrations of the effluent were about 550 and 0 mg L^{-1}, indicating the Fe^0/GAC mixed-potential corrosion reactor had high treatment efficiencies for COD and PO_4^{3-}. After 40 days run, COD concentration of the effluent increased gradually from approximately 550 to 1200 mg L^{-1}, and PO_4^{3-} of the effluent also increased gradually from 0 to about 55 mg L^{-1}, which suggested that the treatment efficiency of the Fe^0/GAC mixed-potential corrosion reactor began to decrease gradually to 0% after 40 days run. In other words, the Fe^0/GAC mixed-potential corrosion reactor would lose its treatment capacity over time (about 90 days). Figure 1b shows the changes of total iron concentration in the effluent of the Fe^0/GAC mixed-potential corrosion reactor with the treatment time increase. During the initial 40 days, the total iron concentration of the effluent was about 35 mg L^{-1}, while the total iron concentration of the effluent decreased gradually to 0 mg L^{-1} in the latter 60 days (from 40th to 100th day), which indicating that the reactivity of sponge iron would be lost gradually due to the corrosion products or other precipitates on the surface of sponge iron (Fe^0). Furthermore, the passive film on the surface of sponge iron (Fe^0) would be formed by the sedimentation of corrosion products or other precipitates, which could restrain the corrosion reaction of iron, so the total iron concentration of the effluent would decrease gradually to 0 mg L^{-1} after long-term run.

3.2. Morphology and Elemental Analysis on the Surface of the Passive Sponge Iron and GAC. According to the aforementioned research results, it was clear that the Fe^0/GAC mixed-potential corrosion reactor would lose its treatment capacity for the pollutants in ABS resin wastewater after long-term run, which might be resulted from the passivation of sponge iron and GAC in Fe^0/GAC mixed-potential corrosion reactor. Therefore, after 100 days continuous run of the Fe^0/GAC mixed-potential corrosion reactor, the morphology and elemental composition of the passive film on the surface of sponge iron (Fe^0) and GAC should be observed and analyzed using SEM and EDS.

It could be seen from the SEM image in Figure 2 that there were many blocks with regular geometry shape which might be the crystalline compounds, and these blocks were distributed randomly in the substrate with an irregular shape on the surface of passive sponge iron (Fe^0). In order to analyze the elementary composition of the passive film on the surface of passive sponge iron (Fe^0), the area (1) and spot (2−5) in the SEM image were analyzed by EDS spectrum (Figure 2). There were four kinds of elements on the surface of passive sponge iron (Fe^0), such as O, P, S, and Fe, and the atomic ratio of the four kinds of elements was 60.04% (O), 4.92% (P), 10.40% (S), and 24.64% (Fe), respectively (Figure 2a). There were only three kinds of elements on the surface of blocks with regular geometry shape, such as O, P, Fe, and the atomic ratio of the three kinds of elements was about 70.59% (O), 14.05% (P), and 15.36% (Fe), respectively (Figure 2bc). It could be speculated that the composition of the blocks with regular geometry might be $FePO_4$ or $Fe_3(PO_4)_2$. As shown in Figure 2d,e, there were only three kinds of elements on the surface of the substrate with irregular shape, such as O, S, Fe, and the atomic ratio of the three kinds of elements was about 33.40% (O), 24.06% (S), and 42.54% (Fe), respectively. It could be speculated that the constituent of the substrate with irregular shape might be FeS, Fe_2O_3, or Fe_3O_4.

Figure S4 in Supporting Information shows the SEM image and EDS spectrum of the passive film on the surface of passive GAC. Comparing the SEM images and EDS spectra of the passive sponge iron (Fe^0) and GAC, it can be seen that the surface morphology and elementary composition of the passive sponge iron (Fe^0) and GAC had a uniform characteristic. In other words, the passive film of the passive sponge iron (Fe^0) and GAC both consisted of the four main elements, O, P, S, and Fe, and the same passive film was formed on the surface of sponge iron (Fe^0) and GAC after 100 days continuous run.

On the surface of passive sponge iron (Fe^0) and GAC, the blocks with regular geometry shape had five different structural forms of cubic structure, laminar structure, stripe structure, radiating structure, and folding structure (see Figure S5, Supporting Information). The different structural forms of the blocks resulted from the different external prestresses for these blocks in the process of growth. The substrate with an irregular shape on the surface of the passive sponge iron (Fe^0) and GAC had indefinable form and porous structure (see Figure S6 in the Supporting Information), which might result from the mixture of FeS, Fe_2O_3, and Fe_3O_4 in the substrate, and the mixture could not form a regular shape under the mutual interference of the three compounds. On the contrary, in some areas on the surface of passive sponge iron (Fe^0) and GAC, there was a smoothing and compact structure passive film which consisted of O, S, and Fe (see Figure S7, Supporting Information). And the atomic ratios of the three kinds of elements were about 16.88% (O), 41.92% (S), and 41.20% (Fe), respectively. Apparently, the atomic ratios of S and Fe were both much higher than that of O, and the atomic ratio of S was almost equal to that of Fe, which indicates that the main compound of this passive film was FeS, and the O element was

dx.doi.org/10.1021/ie203019t | Ind. Eng. Chem. Res. 2012, 51, 7777−7785

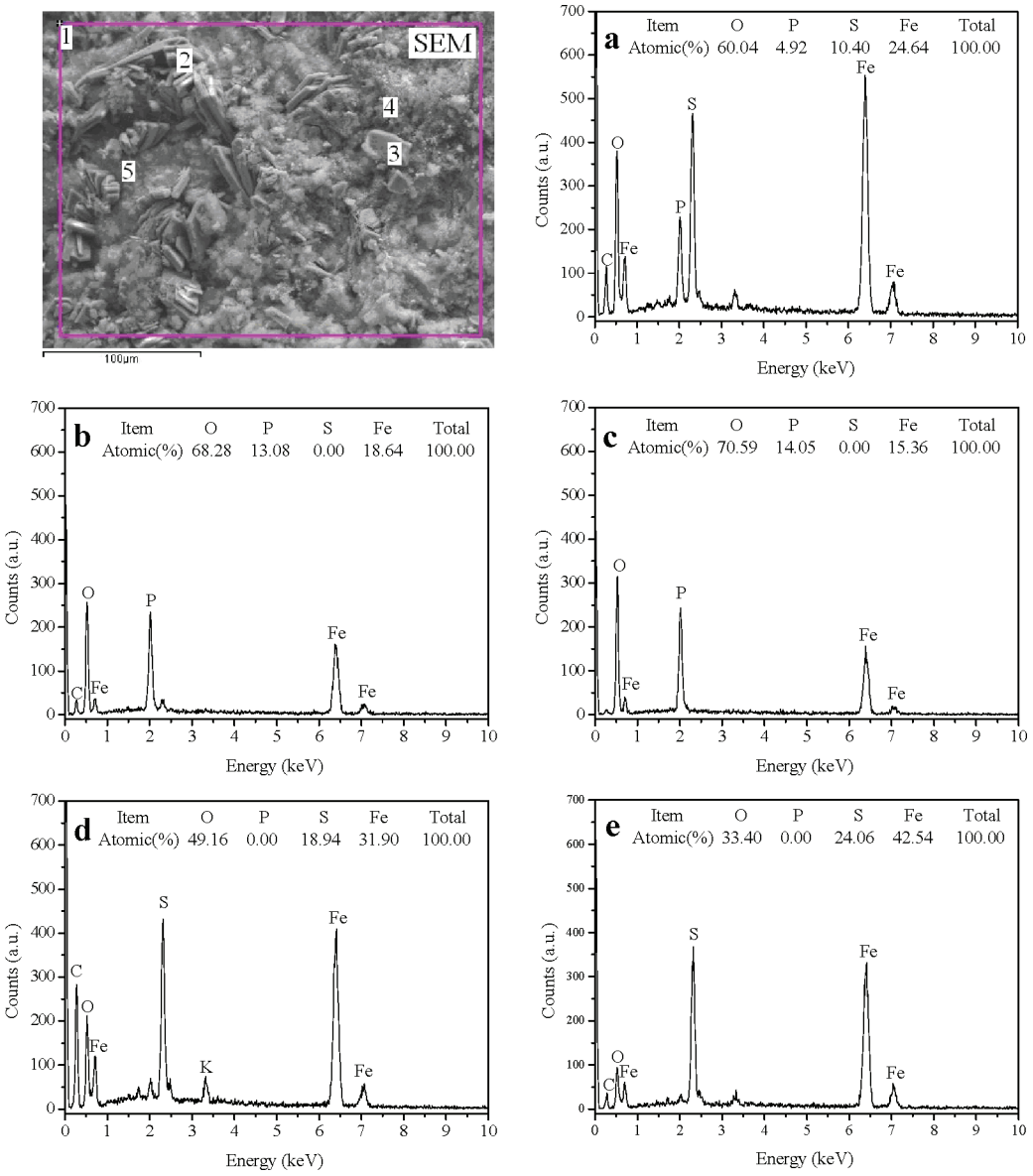

Figure 2. SEM and EDS of the passive sponge iron surface: (a) EDS spectrum of area (1) in the purple frame of the SEM image; (b–e) EDS spectrum of spot (2–5) in the SEM image.

in the form of crystal water. In other words, the passive film mainly containing FeS had a smooth and compact structure without interference of the other compounds.

Therefore, the passive film containing a single compound, such as one of $FePO_4$, $Fe_3(PO_4)_2$, or FeS, had a regular structure (see Figure S5 and Figure S7, Supporting Information). On the contrary, the passive film containing mixture compounds, such as the mixture of FeS, Fe_2O_3, and Fe_3O_4, had an irregular structure (see Figure S6, Supporting Information).

3.3. Cross-Section Characteristics of the Passive Sponge Iron and GAC. To investigate the cross-section characteristics of the passive sponge iron (Fe^0) and GAC, X-ray dot-mapping was used for analyzing the element distribution on the cross-section of the passive sponge iron (Fe^0) and GAC, and SEM was used to analyze the internal morphology of the passive film and packing particles.

The raw sponge iron (Fe^0) and GAC, as a blank control group, were analyzed before the investigation of the passive sponge iron (Fe^0) and GAC. SEM image and X-ray dot-mappings for P, S, Fe, and O of cross sections of raw sponge iron are shown in Figure S8 (Supporting Information). It could be seen from the SEM image (see Figure S8b, Supporting Information) and color mapping of Fe-blue, S-green, and P-red (see Figure S8a, Supporting Information) that there was no passive film on the surface of raw sponge iron, and some pore structure was in the inner part of the raw sponge iron. The P (Figure S8c, Supporting Information), S (Figure S8d), Fe (Figure S8e), and O (Figure S8f) dot-mappings demonstrate that only Fe and minor O were detected on the cross-section of raw sponge iron, and there was no S and P to be found in the inner part of the raw sponge iron. The minor O, which was detected on the cross-section, resulted from the oxidation of iron on the surface of sponge iron and in its internal pore structure by oxygen in air. The SEM and X-ray dot-mapping on the cross-section of raw GAC reveal that there was only C in the GAC (Figure S9, Supporting Information).

dx.doi.org/10.1021/ie203019t | Ind. Eng. Chem. Res. 2012, 51, 7777–7785

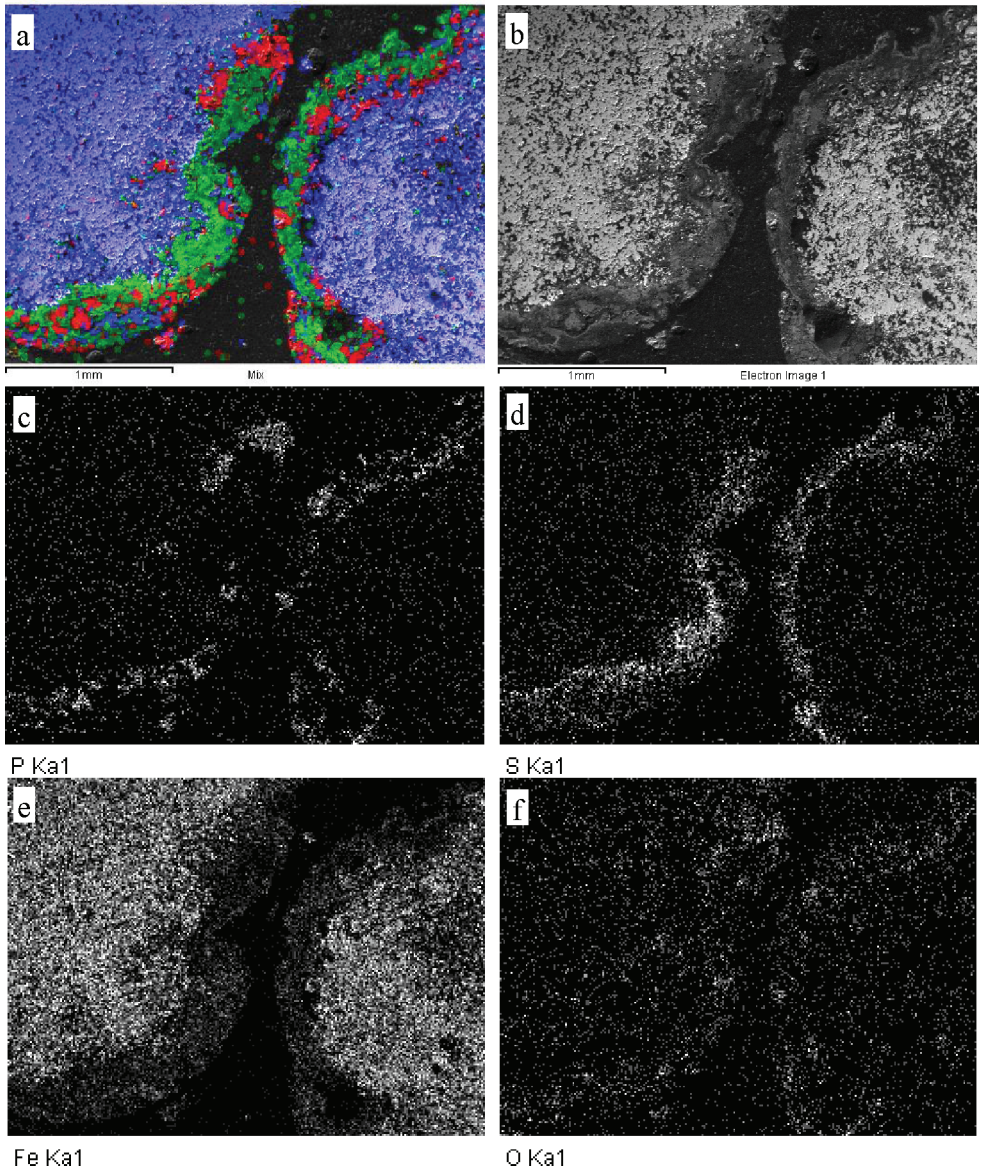

Figure 3. SEM image and X-ray dot-mapping on the cross-section of passive sponge iron: (a) color mappings of three elements (Fe, blue; S, green; and P red) (the black dots were epoxy resins); (b) SEM image; (c–f) X-ray dot-mapping on the cross-section of passive sponge iron, distribution of P, S, Fe, and O.

SEM image and X-ray dot-mappings for P, S, Fe, and O on the cross-section of passive sponge iron are shown in Figure 3. The SEM image (Figure 3b) and color dot-mapping of Fe-blue, S-green, and P-red (Figure 3a) demonstrate that the passive sponge iron (Fe^0) was covered with a passive film with a thickness of 200–600 μm. The X-ray dot-mapping of P (Figure 3c) shows that the P was distributed with a "cluster" block in the passive film, randomly, while the S was distributed uniformly in the passive film (Figure 3d). Apparently, from the color dot-mapping (Figure 3a) of Fe (blue), P (red), and S (green), the P was distributed randomly in the substrate of S with a cluster block. The X-ray dot-mapping (Figure 3e) of Fe reveals that the Fe was distributed uniformly in the passive film, but the amount of Fe in the passive film was much less than that of the inner sponge iron. After 100 days of continuous operation of the Fe^0/GAC mixed-potential corrosion reactor, plenty of Fe was released in the form of Fe^{2+} or Fe^{3+} ions, and the remaining Fe adhered to the surface of the sponge iron (Fe^0) as iron compounds, which formed a thick passive film. Therefore, the amount of Fe in the passive film was much less than that within the sponge iron (Fe^0). The X-ray dot-mapping of O (Figure 3f) shows that O was distributed with a cluster block in the passive film, randomly, and its regularity of distribution was accord with that of P cluster block, which indicated that the O was mainly bonded to the P (such as PO_4^+) and not to S. Therefore, the S was mainly bonded to the Fe (such as FeS), in addition, and the O also could be bonded to the Fe (such as Fe_2O_3 and Fe_3O_4).

From the contrast between EDS spectra on the surface of the passive sponge iron (Figure 2) and X-ray dot-mappings on the cross-section of the passive sponge iron (Figure 3), it was clear that the distribution of Fe, P, S, and O on the surface of the passive film was according to that within the passive film.

As shown in Figure 4 in Supporting Information, it was the SEM image and X-ray dot-mappings of passive GAC. Compared the cross-section characteristics of passive sponge

dx.doi.org/10.1021/ie203019t | *Ind. Eng. Chem. Res.* 2012, 51, 7777–7785

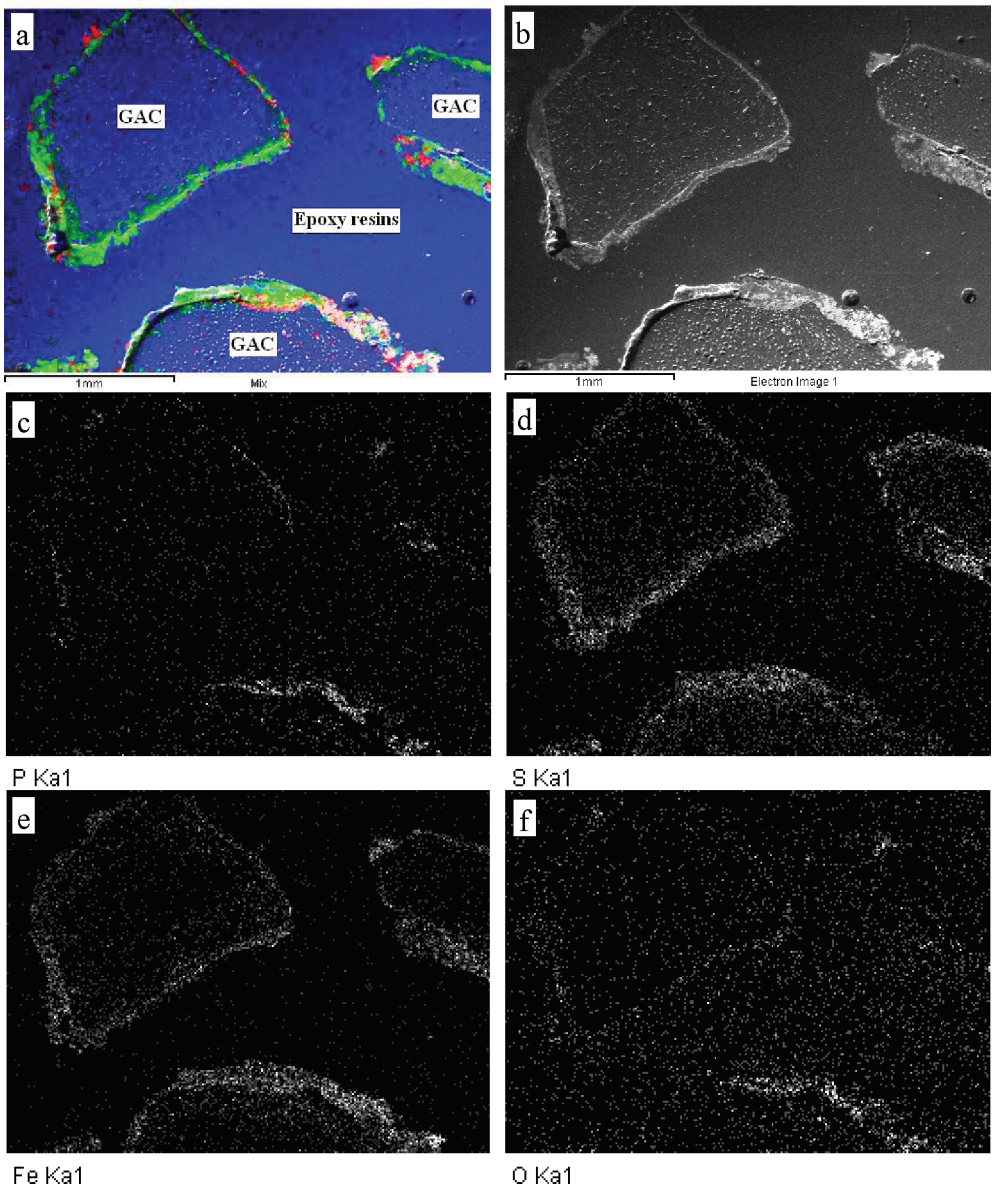

Figure 4. SEM and X-ray dot-mapping on the cross-section of passive GAC: (a) color mapping of three elements (C, blue; S, green; and P, red) (the blue area between GACs was epoxy resins, which contained plenty of C elements.); (b) SEM image; (c–f) X-ray dot-mapping on the cross-section of passive sponge iron, distribution of P, S, Fe, and O.

iron (Figure 3) with that of passive GAC (Figure 4), it was clear that they had the same distribution rule of Fe, P, S and O. In other words, the passive film on the surface of sponge iron and GAC had a same formation process and mechanism.

3.4. Compound Composition of the Passive Film. The elemental composition and distribution in the passive film was seriously investigated by SEM, EDS, and X-ray dot-mapping, but the compound composition of the passive film was not analyzed in detail. The XRD pattern of the passive film of sponge iron and GAC was shown in Figure 5. The XRD data reveals the coexistence of five kinds of compounds in the passive film of sponge iron and GAC. The five kinds of compounds in the passive film were $Fe_3(PO)_2{\cdot}8H_2O$, $FePO_4{\cdot}3H_2O$, Fe_2O_3, Fe_3O_4, and FeS (see Table S2, Supporting Information), respectively, which were in accord with the aforementioned conjecture by EDS and X-ray dot-mapping. In addition, there was crystalline carbon in the passive film of sponge iron, which was from two aspects: one was the remaining carbon after the iron loss of sponge iron by corrosive action, and the other was from GAC by the contact of sponge iron and GAC. The crystalline carbon and amorphous carbon detected in the passive film of GAC were from GAC itself. In general, the activated carbon consists of crystalline carbon and amorphous carbon.

3.5. Formation Mechanism of the Compounds in Passive Film. Characteristics of the passive sponge iron and GAC were investigated seriously by SEM, EDS, and XRD, which revealed that the formation of passive film on the packing particles in the Fe^0/GAC mixed-potential corrosion reactor after long-term running would obstruct the formation of macroscopic galvanic cells between sponge iron (Fe^0) and GAC and decrease the treatment efficiency of the Fe^0/GAC mixed-potential corrosion reactor. To obstruct the formation of passive film and retain the high treatment efficiency of the Fe^0/GAC mixed-potential corrosion reactor, the formation mechanism of the compounds in the passive film should be investigated first, which was the precondition for the control of

dx.doi.org/10.1021/ie203019t | Ind. Eng. Chem. Res. 2012, 51, 7777–7785

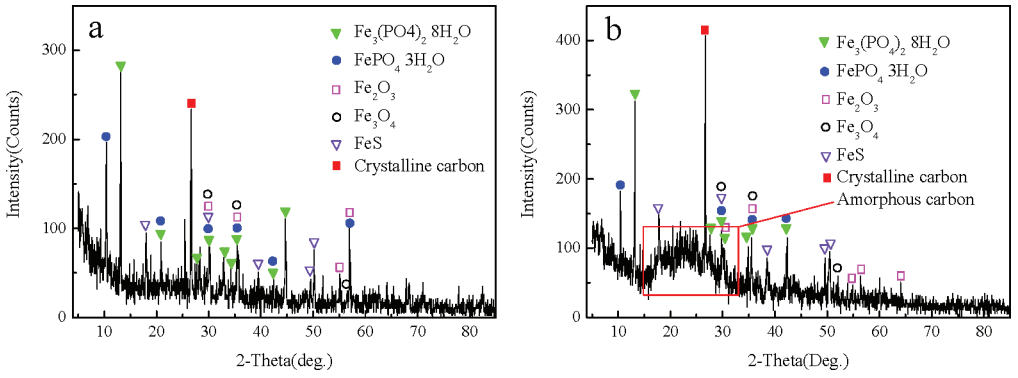

Figure 5. XRD patterns of passive film on the surface of sponge iron (a) and GAC (b).

the passivation of packing particles in the Fe^0/GAC mixed-potential corrosion reactor.

The passive film mainly consists of five kinds of compounds such as $Fe_3(PO_4)_2{\cdot}8H_2O$, $FePO_4{\cdot}3H_2O$, FeS, Fe_2O_3, and Fe_3O_4. The formation mechanism of passive film could be deduced from the aforementioned analysis results and half-cell reactions of the Fe^0/GAC mixed-potential corrosion reactor.[17] The formation mechanism of $Fe_3(PO_4)_2{\cdot}8H_2O$, $FePO_4{\cdot}3H_2O$, FeS, Fe_2O_3, and Fe_3O_4 can be detailed as shown in what follows, $C_aH_bO_cN_d$ stands for the main pollutants in ABS resin wastewater. [H], Fe^{2+}, and Fe^{3+} were produced from the macroscopic galvanic cells and microscopic galvanic cells in Fe^0/GAC mixed-potential corrosion reactor. The pollutants with higher redox potential could be decomposed into the smaller organic molecules by free hydrogen radicals [H], and H^+ and O^{2-} byproducts were produced in this process. Thus, the Fe^{2+} and Fe^{3+} were bonded with O^{2-}, and produced Fe_2O_3 and Fe_3O_4, respectively. In ABS resin wastewater, the PO_4^{3+} ion concentration was about 50−60 mg L^{-1}, which could react quickly with Fe^{2+} and Fe^{3+} to form $Fe_3(PO_4)_2{\cdot}8H_2O$ and $FePO_4{\cdot}3H_2O$, respectively. SO_4^{2+} ion might be reduced to S^{2-} by the strong reduction of free hydrogen radicals [H], and the S^{2-} could react with Fe^{2+} to form FeS. The five compounds of $Fe_3(PO_4)_2{\cdot}8H_2O$, $FePO_4{\cdot}3H_2O$, FeS, Fe_2O_3, and Fe_3O_4 were deposited on the surface of sponge iron (Fe^0) and GAC by coprecipitation, which formed a strong passive film on the surface of packing particles in the Fe^0/GAC mixed-potential corrosion reactor. And the formation of passive film was mainly resulted from the elements of S and P, which were from the SO_4^{2-} and PO_4^{3-} in ABS resin wastewater. Therefore, in order to retain the high treatment efficiency of the Fe^0/GAC mixed-potential corrosion reactor and prolong its operating life, the inorganic ions in wastewater, especially for SO_4^{2-} and PO_4^{3-}, should be removed first.

$$Fe - 2e^- \rightarrow Fe^{2+} \quad (5)$$

$$Fe^{2+} - e^- \rightarrow Fe^{3+} \quad (6)$$

$$2H^+ + 2e^- \rightarrow 2[H] \rightarrow H_2\uparrow \quad (7)$$

$$2[H] + C_aH_bO_cN_d \rightarrow C_aH_{b+2}O_{c-1}N_d + O^{2-} \rightarrow C_aH_bO_{c-1}N_d + O^{2-} + 2H^+ \quad (8)$$

$$4O^{2-} + Fe^{2+} + 2Fe^{3+} \rightarrow Fe_3O_4\downarrow \quad (9)$$

$$3O^{2-} + 2Fe^{3+} \rightarrow Fe_2O_3\downarrow \quad (10)$$

$$PO_4^{3-} + Fe^{2+} + 8H_2O \rightarrow Fe_3(PO_4)_2{\cdot}8H_2O\downarrow \quad (11)$$

$$PO_4^{3-} + Fe^{3+} + 3H_2O \rightarrow FePO_4{\cdot}3H_2O\downarrow \quad (12)$$

$$8[H] + SO_4^{2-} \rightarrow S^{2-} + 4H_2O \quad (13)$$

$$Fe^{2+} + S^{2-} \rightarrow FeS\downarrow \quad (14)$$

3.6. Surface Physical Properties of the Sponge Iron and GAC. The surface area and total pore volume of raw sponge iron were 8.10 $m^2\ g^{-1}$ and 0.009 mL g^{-1} (see Table S3, Supporting Information), respectively, which revealed that there was no fine pore structure on the surface of the raw sponge iron. However, the surface area and total pore volume of sponge iron was increased to 28.66 $m^2\ g^{-1}$ and 0.029 mL g^{-1} after passivation, respectively, which resulted from the formation of porous passive film (Figure S6, Supporting Information). It is clear that the surface area and total pore volume of GAC was decreased from 748.06 $m^2\ g^{-1}$ and 0.481 mL g^{-1} to 383.81 $m^2\ g^{-1}$ and 0.255 mL g^{-1} after passivation (Table S3, Supporting Information), respectively, which suggests that the fine pore structure on the surface of GAC was obstructed by the passive film.

Figure 6 shows the nitrogen adsorption isotherms for sponge iron and GAC before and after passivation. It is evident from

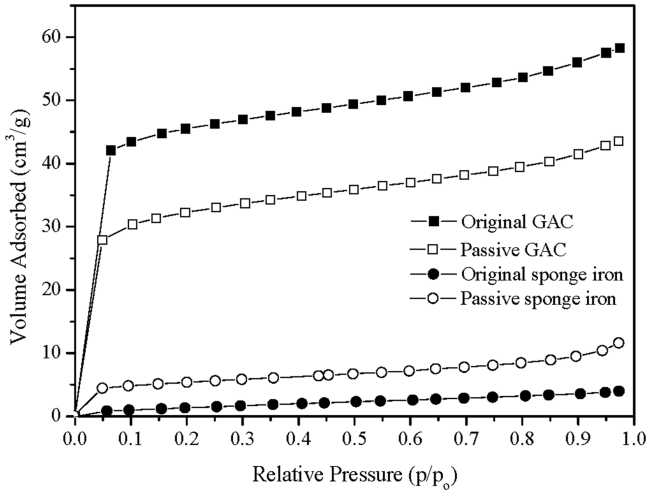

Figure 6. Nitrogen adsorption isotherms for the GAC and sponge iron before and after passivation.

Figure 6 that after the formation of passive film, the amount of nitrogen adsorbed decreases obviously for GAC, but the

dx.doi.org/10.1021/ie203019t | Ind. Eng. Chem. Res. 2012, 51, 7777−7785

amount of nitrogen adsorbed increases a little for sponge iron. It is also obvious that after the formation of passive films, the shape of the isotherm of sponge iron turns from type II to type I with the monolayer completed at $p/p_0 < 0.6$. The slight nitrogen uptake at higher relative pressure reveals that a slight micropore filling occurs at lower relative pressure, and multilayer adsorption and condensation are predominant on the macroporous structure at higher relative pressure. In other words, there were micropores and macropores in the passive film, which was in agreement with the SEM image of the passive film (Figure S6, Supporting Information). After the formation of passive film, the amount of nitrogen adsorbed decreases for GAC, but the shape of its isotherm did not change (remaining type II), which suggested the passive film did not obstruct all micropores of GAC, and the nitrogen could pass through the passive film to the surface of GAC by the micropores and macropores of the passive film.

A relevant relationship exists between the porosity and surface area. As the porosity increases, the surface area increases especially for the materials with high microporosity since the microporous structure has the majority of the surface area. Figure 7 shows the pore size distribution (PSD) for the sponge

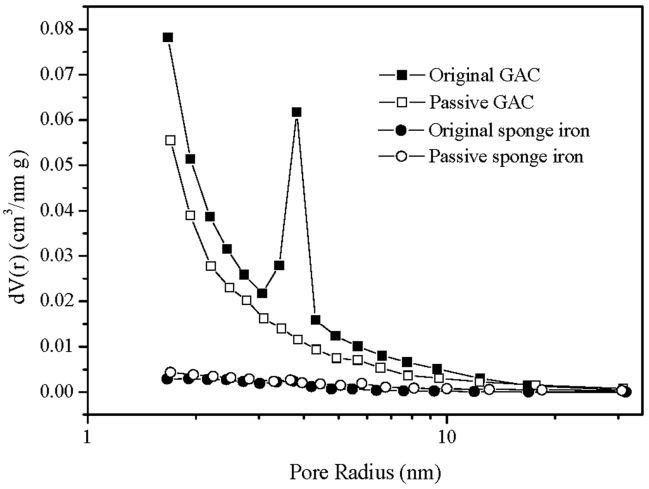

Figure 7. Pore size distribution for the GAC and sponge iron before and after passivation.

iron and GAC before and after passivation calculated by the BJH method using desorption isotherms. The raw GAC exhibits a maximum, which extends toward the pore of 4 nm (Figure 7). This steep increase of the PSD toward the micropore region corresponds to the high BET surface area in the raw GAC. In other words, the reduction of the BET surface area for the passive GAC results from the obstruction of the 4 nm pores by the passive film. In addition, the raw sponge iron and passive sponge iron both only have small micropores (pore size <10 nm) (Figure 7).

In a word, after the formation of a passive film, the majority of the micropores of GAC was obstructed which resulted in the reduction of adsorptive capacity for GAC. Furthermore, the reduction of adsorptive capacity for GAC would decrease the resistance to the shock loadings of toxic refractory wastewater for Fe^0/GAC mixed-potential corrosion reactor.

4. CONCLUSION

After 40 days run, COD concentration of the effluent increased gradually from approximately 550 to 1200 mg L^{-1}, and PO_4^{3-} of the effluent also increased gradually from 0 to about 55 mg L^{-1}, in addition, total iron concentration of the effluent decreased from 35 to 0 mg L^{-1}, which suggested that the Fe^0/GAC mixed-potential corrosion reactor would lose its treatment capacity over time (about 90 days). In the passive film of passivation packing particles, five compounds, $Fe_3(PO)_2 \cdot 8H_2O$, $FePO_4 \cdot 3H_2O$, Fe_2O_3, Fe_3O_4, and FeS, were detected by SEM, EDS, X-ray dot-mapping, and XRD, which obstruct the formation of macroscopic galvanic cells between Fe^0 and GAC and decrease the wastewater treatment efficiency of Fe^0/GAC mixed-potential corrosion reactor. Furthermore, the passivation of Fe^0 and GAC mainly resulted from the inorganic ions in wastewater, especially for SO_4^{2-} and PO_4^{3-}. The surface area and total pore volume of GAC was decreased from 748.06 m^2 g^{-1} and 0.481 mL g^{-1} to 383.81 m^2 g^{-1} and 0.255 mL g^{-1} after passivation, respectively, which suggests that the fine pore structure on the surface of GAC was obstructed by the passive film.

■ ASSOCIATED CONTENT

Ⓢ Supporting Information

Additional information as described in the text. This material is available free of charge via the Internet at http://pubs.acs.org.

■ AUTHOR INFORMATION

Corresponding Author

*E-mail: laibo1981@163.com. Tel./Fax: +86028 85405534.

Author Contributions

The authors declare no competing financial interest.

Notes

The authors declare no competing financial interest.

■ ACKNOWLEDGMENTS

The research is supported by the special S&T project on treatment and control of water pollution (No. 2008ZX07207-004).

■ REFERENCES

(1) Qian, B. Z. Market analysis on domestic and overseas ABS resin. *China Rubber/Plast. Technol. Equip.* **2008**, *34*, 30.

(2) Xu, F. B.; Han, Q. Global market status and prospective analysis of ABS resin. *China Plast. Ind.* **2006**, *34*, 13.

(3) Lin, C. K.; Tsai, T. Y.; Liu, J. C.; Chen, M. C. Enhance biodegradation of petrochemical wastewater using ozonation and bac advanced treatment system. *Water Res.* **2001**, *35*, 699.

(4) Sheng, H. L.; Ching, H. W. Ozonation of phenolic wastewater in a gas-induced reactor with a fixed granular activated carbon bed. *Ind. Eng. Chem. Res.* **2003**, *42*, 1648.

(5) Martins, R. C.; Quinta-Ferreira, R. M. Screening of ceria-based and commercial ceramic catalysts for catalytic ozonation of simulated olive mill wastewaters. *Ind. Eng. Chem. Res.* **2009**, *48*, 1196.

(6) Chen, Y. H.; Chang, C. Y.; Chen, C. C.; Chiu, C. Y.; Yu, Y. H.; Chiang, P. C.; Chang, C. F.; Ku, Y. Decomposition of 2-mercaptothiazoline in an aqueous solution by ozonation with UV radiation. *Ind. Eng. Chem. Res.* **2004**, *43*, 1932.

(7) Pimentel, M.; Oturan, N.; Dezotti, M.; Oturan, M. A. Phenol degradation by advanced electrochemical oxidation process electro-Fenton using a carbon felt cathode. *Appl. Catal B: Environ.* **2008**, *83*, 140.

(8) Yuan, S. H.; Fan, Y.; Zhang, Y. C.; Tong, M.; Liao, P. Pd-catalytic in situ generation of H_2O_2 from H_2 and O_2 produced by water electrolysis for the efficient electro-Fenton degradation of rhodamine B. *Environ. Sci. Technol.* **2011**, *45*, 8514.

(9) Oturan, N.; Zhou, M. H.; Oturan, M. A. Metomyl degradation by electro-Fenton and electro-Fenton-like processes: A kinetics study of the effect of the nature and concentration of some transition metal ions as catalyst. *J. Phys. Chem. A* **2010**, *114*, 10605.
(10) Fockedey, E.; Lierde, A. V. Coupling of anodic and cathodic reactions for phenol electro-oxidation using three-dimensional electrodes. *Water Res.* **2002**, *36*, 4169.
(11) Fan, L.; Ni, J. R.; Wu, Y. J.; Zhang, Y. Y. Treatment of bromoamine acid wastewater using combined process of micro-electrolysis and biological aerobic filter. *J. Hazard. Mater.* **2009**, *162*, 1204.
(12) Lee, J. W.; Cha, D. K.; Oh, Y. K.; Ko, K. B.; Song, J. S. Zero-valent iron pretreatment for detoxifying iodine in liquid crystal display (LCD) manufacturing wastewater. *J. Hazard. Mater.* **2009**, *164*, 67.
(13) Mu, Y.; Yu, H. Q.; Zheng, J. C.; Zhang, S. J. Reductive degradation of nitrobenzene in aqueous solution by zero-valent iron. *Chemosphere* **2004**, *54*, 789.
(14) Ma, L.; Zhang, W. X. Enhanced biological treatment of industrial wastewater with bimetallic zero-valent iron. *Environ. Sci. Technol.* **2008**, *42*, 5384.
(15) Kallel, M.; Belaid, C.; Mechichi, T.; Ksibi, M.; Elleuch, B. Removal of organic load and phenolic compounds from olive mill wastewater by Fenton oxidation with zero-valent iron. *Chem. Eng. J.* **2009**, *150*, 391.
(16) Lai, P.; Zhao, H. Z.; Zeng, M.; Ni, J. R. Study on treatment of coking wastewater by biofilm reactors combined with zero-valent iron process. *J. Hazard. Mater.* **2009**, *162*, 1423.
(17) Cheng, H. F.; Xu, W. P.; Liu, J. L.; Wang, H. J.; He, Y. Q.; Chen, G. Pretreatment of wastewater from triazine manufacturing by coagulation, electrolysis, and internal microelectrolysis. *J. Hazard. Mater.* **2007**, *164*, 385.
(18) Lai, B.; Zhou, Y. X.; Qin, H. K.; Wu, C. Y.; Pang, C. C.; Lian, Y.; Xu, J. X. Pretreatment of wastewater from acrylonitrile−butadiene−styrene (ABS) resin manufacturing by microelectrolysis. *Chem. Eng. J.* **2012**, *179*, 1.
(19) Yang, Y. P.; Xu, X. H.; Chen, H. F. Treatment of chitin-producing wastewater by microelectrolysis-contact oxidization. *J. Zhejiang Univ. Sci.* **2004**, *5*, 436.
(20) Van, D. Z. F. P.; Bisschops, I. A. E.; Lettinga, G.; Field, J. A. Activated carbon as an electron acceptor and redox mediator during the anaerobic biotransformation of azo dyes. *Environ. Sci. Technol.* **2003**, *37*, 402.
(21) Liu, H. N.; Li, G. T.; Qu, J. H.; Liu, H. J. Degradation of azo dye Acid Orange 7 in water by Fe^0/granular activated carbon system in the presence of ultrasound. *J. Hazard. Mater.* **2007**, *144*, 180.